Available online at www.sciencedirect.com

ScienceDirect

IFAC Papers Online CONFERENCE PAPER ARCHIVE

IFAC-PapersOnLine 48-8 (2015) 240–247

Generalizing ODE modeling structure for multivariate systems with distributed parameters

Naim Bajcinca * **Steffen Hofmann** ** **Holger Eisenschmidt** ***
Kai Sundmacher *,***

* *Max Planck Institute, Sandtorstr 1, 39106 Magdeburg*
** *Technische Universität Berlin, Einsteinufer 17, 10587 Berlin*
*** *Otto-von-Guericke Universität, Universitätspl. 2, 39106 Magdeburg*

Abstract: We propose an approximate model in form of a system of ordinary differential equations (ODEs) for a class of first-order multivariate linear partial differential equations (PDEs) of the hyperbolic type. The resulting scheme utilizes the method of moments and least-square approximations over orthogonal polynomial bases for the factors of PDE depending on the spatial coordinate of the PDE. The class of examined PDEs appears typically in population balance systems with fines removal. The proposed modeling approach is generally of interest for control and optimization of multivariate systems with distributed parameters.

Keywords: multi-variate processes, population balance systems, method of moments, systems with distributed parameters, orthogonal polynomials, crystallization

1. INTRODUCTION

The present paper is devoted to design of an approximate ODE modeling scheme for multi-variate first-order hyperbolic partial differential equations (PDEs) of the form:

$$\partial_t f(\boldsymbol{x},t)+\partial_{\boldsymbol{x}}^T \boldsymbol{G}(\boldsymbol{x},t)f(\boldsymbol{x},t)+h(\boldsymbol{x})f(\boldsymbol{x},t)=B(t)\delta(\boldsymbol{x}), \quad (1a)$$

with given initial condition $f(\boldsymbol{x},0) = f_0(\boldsymbol{x})$, and notational conventions: $\boldsymbol{x} = (x_1 \dots x_n)^T$, $\partial_t = \partial/\partial t$, $\partial_i = \partial/\partial x_i$, $\partial_{\boldsymbol{x}}^T = (\partial_1, \cdots, \partial_n)$, $\boldsymbol{G}(\boldsymbol{x},t) = (G_1, \cdots, G_n)^T$ and $\delta(\boldsymbol{x}) = \prod_{i=1}^n \delta(x_i)$. Furthermore, we assume separability conditions for the decaying and growth rate terms:

$$h(\boldsymbol{x}) = \textstyle\prod_{i=1}^n h_i(x_i), \quad (1b)$$
$$G_i(\boldsymbol{x},t) = \gamma_i(x_i)G_{0,i}(t). \quad (1c)$$

A variety of corresponding numerical schemes exist in the engineering and applied mathematics literature, including the finite difference schemes, the high-resolution finite volume methods (Koren, 1993), quadrature method of moments (Qamar et al., 2006), and many other. A main impetus of the majority of these contributions has been enhancement of efficiency, accuracy and robustness of integration schemes. Our approach, in a series of previous articles, has however consisted in the design of approximating models in form of various structures of systems of ordinary differential equations (ODEs) based on the standard method of moments. In particular, in the previous work (Bajcinca et al., 2014), we proposed such solutions based on polynomial approximations of the terms $\gamma_i(x_i) > 0, x > 0$, for the sub-class of systems (1a) with $h_i(x_i) \equiv 0$. The present work is an extension thereof, where the functions $h_i(x_i)$ are assumed to be arbitrary continuous functions accepting an expansion over a polynomial space.

The PDE (1) appears frequently in population balance systems. In the source term on the right-hand side of Eq. (1a), $B(t)$ stands for the birthrate function, and $\delta(\boldsymbol{x})$ is the Dirac function, suggesting that new population ingredients are born at a negligible size. The function $f(\boldsymbol{x},t)$ represents the population density function defined as the number of particles per unit volume in the property space, i.e., the net number of particles is given by $\int_{\mathbb{R}^n} f(\boldsymbol{x},t)\mathrm{d}\boldsymbol{x}$, and $f_0(\boldsymbol{x})$ stands for the given initial density function. The PDE (1a) is furthermore usually coupled to conservation laws and additional algebraic kinetic equations, providing a dynamic feedback via integral terms (i.e., the moments of $f(\boldsymbol{x},t)$) into the birthrate $B(t)$ and growth factors $G_{0,i}$. For gaining an insight into the role of the filtering term $h(\boldsymbol{x})$ in the equation (1a), let e.g. $n = 1$, $G_{0,1} = 0$ and $B = 0$, this leading to: $\mathrm{d}f(x,t)/\mathrm{d}t + h(x)f(x,t) = 0$. For $x > 0$ and $h(x) > 0$, the function $f(x,t)$ will then decay in time due to the presence of the factor $h(x)$, which we, hence, denote as decaying or filtering term.

A prominent application of population balance systems (Ramkrishna, 2000), where our scheme appears to be particularly useful is found in the context of multivariate batch crystallization. Crystallization processes are widely used in chemical production systems for separation and purification purposes. To overcome issues related to unwanted nucleation and the difficulties resulting thereof in further downstream processes, such as filtration or drying, an external fines removal loop is frequently applied. This technique ensures a significant reduction of the fines and the problems associated with the nucleation. As such operations in batch crystallization are commonly modeled by a decaying term $h(\boldsymbol{x},t) > 0$ within a certain range of size $\boldsymbol{x} \leq \boldsymbol{x}_{\max}$ in the property space as in (1a), our model is, additionally, of main interest in control of multivariate crystallization processes, and, more generally, of the PDEs of the form (1a). Results related to the case $h(\boldsymbol{x}) \equiv 0$ can be found, e.g., in (Bajcinca, 2013), while their extension to the underlying class (1a) is a matter of future work.

Peer review under responsibility of International Federation of Automatic Control.
10.1016/j.ifacol.2015.08.188

2. GENERALIZED METHOD OF MOMENTS

We begin with an often used transformation of property space $\boldsymbol{x} \to \boldsymbol{\lambda}$ to drop the γ_i-terms from the PDE (1a), and a proper scaling of the distribution function $f(\boldsymbol{x}, t)$, (see, e.g., Bajcinca et al., 2014):

$$\frac{\mathrm{d}\lambda_i}{\mathrm{d}x_i} = \frac{1}{\gamma_i(x_i)}, \quad \text{i.e.,} \quad \lambda_i(x_i) = \int_0^{x_i} \frac{\mathrm{d}\zeta}{\gamma_i(\zeta)}, \tag{2a}$$

$$\tilde{f}(\boldsymbol{\lambda}, t) := f(\boldsymbol{x}(\boldsymbol{\lambda}), t) \prod_{i=1}^n \gamma_i(x_i(\lambda_i)). \tag{2b}$$

The functions $\lambda_i(x_i)$ are monotonous with well-defined inverses $x_i(\lambda_i)$. With $x_i(0) = 0$ and $\frac{\mathrm{d}x_i}{\mathrm{d}\lambda_i} = \gamma_i(x_i)$, we have:

$$\delta(\boldsymbol{x}(\boldsymbol{\lambda})) = \frac{\delta(\boldsymbol{\lambda})}{\prod_{i=1}^n \gamma_i(0)}, \quad \gamma_i(0) \neq 0.$$

With these substitutions, and the identity $\gamma_i(x_i)\delta(x_i) = \gamma_i(0)\delta(x_i)$, the PDE (1a) simplifies in that it gets free of the size-dependent growth rate terms:

$$\partial_t \tilde{f}(\boldsymbol{\lambda}, t) + \partial_{\boldsymbol{\lambda}}^T \boldsymbol{G_0}(t) \tilde{f}(\boldsymbol{\lambda}, t) + h(\boldsymbol{\lambda}) \tilde{f}(\boldsymbol{\lambda}, t) = B(t)\delta(\boldsymbol{\lambda}), \tag{3a}$$

where, with a slight abuse of notation, we adopt: $\gamma_i(\lambda_i) := \gamma(x_i(\lambda_i))$ and $h_i(\lambda_i) := h_i(x_i(\lambda_i))$. Then:

$$\tilde{f}(\boldsymbol{\lambda}, 0) = f_0(\boldsymbol{x}(\boldsymbol{\lambda})) \prod_{i=1}^n \gamma_i(\lambda_i), \tag{3b}$$

$$h(\boldsymbol{\lambda}) = \prod_{i=1}^n h_i(\lambda_i), \tag{3c}$$

$$\boldsymbol{G_0}(t) = (G_{0,1}, \cdots, G_{0,n})^T, \tag{3d}$$

and, additionally, it holds: $\tilde{f}(\boldsymbol{\lambda}, t) = \tilde{f}(\lambda_1, \ldots, \lambda_n, t)$, $\boldsymbol{\lambda} = (\lambda_1, \ldots, \lambda_n)^T$, $\partial_i = \partial/\partial\lambda_i$, $\partial_{\boldsymbol{\lambda}}^T = (\partial_1, \cdots, \partial_n)$, etc.

Referring to the method of moments, we introduce the moments of the original distribution function $f(\boldsymbol{x}, t)$ as

$$\mu_{i_1 \ldots i_n}(t) = \int_{\mathbb{R}^n} x_1^{i_1} \ldots x_n^{i_n} f(\boldsymbol{x}, t)\, \mathrm{d}\boldsymbol{x}, \tag{4}$$

were $i_1, \ldots, i_n = 0, 1, 2, etc.$ With regard to the mass-balance law and the kinetics of the particulate process, in particulate systems, the moments $\mu_{i_1 \ldots i_n}$ invoke frequently an intrinsic feedback action into the PDE (3a) via integral terms such as the volume V_C that can be expressed in form of a linear combination thereof. Its definition reads:

$$V_C(t) = \int_{\mathbb{R}^n} \eta(\boldsymbol{x}) f(\boldsymbol{x}, t)\, \mathrm{d}\boldsymbol{x} = \int_{\mathbb{R}^n} \eta(\boldsymbol{\lambda}) \tilde{f}(\boldsymbol{\lambda}, t)\, \mathrm{d}\boldsymbol{\lambda}, \tag{5a}$$

where $\eta(\boldsymbol{x})$ denotes the volume of a single particle, and, we adopt the notational convention: $\eta(\boldsymbol{\lambda}) = \eta(\boldsymbol{x}(\boldsymbol{\lambda}))$. Regular particles exhibit multivariate polynomial expression of the volume $\eta(\boldsymbol{x}) = \eta(x_1, \ldots, x_n)$. For instance, in case of bivariate particles, we have:

$$\eta(\lambda_1, \lambda_2) = \sum\nolimits_{i+j=3} \alpha_{ij} x_1^i(\lambda_1) x_2^j(\lambda_2). \tag{5b}$$

In particulate systems, the time dependence of the term $B(t)$ and $G_{0,i}(t)$ in the PDE (3a) is rather implicit and is determined by the evolution of the volume term V_C, as well as some external input variable u in form of nonlinear algebraic equations:

$$B = B(u, V_C) \quad \text{and} \quad G_{0,i} = G_{0,i}(u, V_C). \tag{6}$$

Following the approach of Bajcinca et al. (2014), in this section, we introduce the ODE approximate structure for the PDE (3a). To this end, we invoke polynomial approximations over a given sequence of polynomials $\phi_k(\lambda)$, $k = 0, 1, 2, etc$, for the factors $x^i(\lambda)$ (appearing in the integrand of (4)):

$$x^i(\lambda) \approx \sum_{k=0}^p b_{ki} \phi_k(\lambda), \tag{7a}$$

as well as for the products $h(\lambda)\phi_i(\lambda)$:

$$h(\lambda)\phi_i(\lambda) \approx \sum_{k=0}^p d_{ki} \phi_k(\lambda), \quad i = 0 \ldots p \tag{7b}$$

where, for simplicity, we drop the coordinate indices $i_1, \ldots, i_n$, and we let the corresponding p's be sufficiently large. The parameters b_{ki} and d_{ki} in (7) depend on the chosen polynomial basis. The simplest basis is given by the monomials $\phi_i(\lambda) = \lambda^i$, which lead to the so-called eigenmoments, that have been studied in earlier works of the authors, (see Bajcinca et al., 2014, for details). For any basis, appropriate constants c_{ki} satisfying

$$\frac{\mathrm{d}}{\mathrm{d}\lambda}\phi_i(\lambda) = \sum_{k=0}^{i-1} c_{ki} \phi_k(\lambda), \quad i = 0, 1, 2, etc \tag{7c}$$

are uniquely defined and can be easily computed. Next, introduce the generalized moments corresponding to the scaled density function $\tilde{f}(\lambda, \tau)$:

$$\nu_{j_1 \ldots j_n}(t) = \int_{\mathbb{R}^n} \phi_{j_1}(\lambda_1) \ldots \phi_{j_n}(\lambda_n) \tilde{f}(\boldsymbol{\lambda}, t)\, \mathrm{d}\boldsymbol{\lambda}, \tag{8}$$

where $j_i = 0, 1, \ldots, p_i$ and $i = 1, \ldots, n$. To avoid complex expressions, the forthcomming deliberations are confined to the bivariate case, i.e. to $n = 2$. Then, by applying the rule of integration by parts and Eqs. (7), we have:

$$\begin{aligned}
\frac{\mathrm{d}}{\mathrm{d}t}\nu_{ij} &= \int_0^\infty \int_0^\infty \phi_i(\lambda_1)\phi_j(\lambda_2)\partial_t \tilde{f}(\lambda_1, \lambda_2, t)\mathrm{d}\lambda_1\lambda_2 \\
&\quad - G_{0,2} \int_0^\infty \phi_i(\lambda_1)\mathrm{d}\lambda_1 \int_0^\infty \phi_j(\lambda_2)\partial_2 \tilde{f}\mathrm{d}\lambda_2 \\
&\quad - \int_0^\infty h_1(\lambda_1)\phi_i(\lambda_1)\mathrm{d}\lambda_1 \int_0^\infty h_2(\lambda_2)\phi_j(\lambda_2)\tilde{f}\mathrm{d}\lambda_2 \\
&= \phi_i(0)\phi_j(0)B(t) + G_{0,1} \int_0^\infty \int_0^\infty \tilde{f} \frac{\mathrm{d}\phi_i}{\mathrm{d}\lambda_1}\phi_j(\lambda_2)\mathrm{d}\lambda_1\mathrm{d}\lambda_2 \\
&\quad + G_{0,2} \int_0^\infty \int_0^\infty \tilde{f}\phi_i(\lambda_1)\frac{\mathrm{d}\phi_j}{\mathrm{d}\lambda_2}\mathrm{d}\lambda_1\mathrm{d}\lambda_2 \\
&\quad - \int_0^\infty h_1(\lambda_1)\phi_i(\lambda_1)\mathrm{d}\lambda_1 \int_0^\infty h_2(\lambda_2)\phi_j(\lambda_2)\tilde{f}\mathrm{d}\lambda_2 \\
&\approx \phi_i(0)\phi_j(0)B(t) + G_{0,1} \sum_{k=0}^{i-1} c_{ki}^{(1)} \int_0^\infty \int_0^\infty \tilde{f}\phi_k\phi_j\mathrm{d}\lambda_1\mathrm{d}\lambda_2 \\
&\quad + G_{0,2} \sum_{l=0}^{j-1} c_{lj}^{(2)} \int_0^\infty \int_0^\infty \tilde{f}\phi_i\phi_l\mathrm{d}\lambda_1\mathrm{d}\lambda_2 \\
&\quad - \int_0^\infty \sum_{k=0}^{i-1} d_{ki}^{(1)}\phi_k(\lambda_1)\mathrm{d}\lambda_1 \int_0^\infty \sum_{l=0}^{j-1} d_{lj}^{(2)}\phi_l(\lambda_2)\tilde{f}\mathrm{d}\lambda_2.
\end{aligned}$$

Hence, we obtain the following ODE computational scheme for the generalized eigenmoments ν_{ij}, $i, j \geq 0$:

$$\begin{aligned}
\dot{\nu}_{ij} &= \phi_i(0)\phi_j(0)\, B(t) \\
&\quad + G_{0,1}(t) \sum\nolimits_{k=0}^{i-1} c_{ki}^{(1)} \nu_{kj}(t) + G_{0,2}(t) \sum\nolimits_{l=0}^{j-1} c_{lj}^{(2)} \nu_{il}(t) \\
&\quad - \sum\nolimits_{k=0}^{p_1} \sum\nolimits_{l=0}^{p_2} d_{ki}^{(1)} d_{lj}^{(2)} \nu_{kl}(t),
\end{aligned} \tag{9}$$

where $c_{ki}^{(1)}$, $c_{lj}^{(2)}$, $d_{ki}^{(1)}$, $d_{lj}^{(2)}$ correspond in an obvious manner to the approximation parameters in the expansion equations (7). The relationship of the generalized moments ν_{kl} to the monomial ones μ_{ij} follows now directly from (7a):

$$\mu_{ij}(t) \approx \sum\nolimits_{k=0,l=0}^{p_1,p_2} b_{ki}^{(1)} b_{lj}^{(2)} \nu_{kl}(t), \tag{10}$$

where p_1 and p_2 are assumed to be sufficiently large. With reference to Eq. (5b), we finally have:

$$V_C(t) = \sum\nolimits_{i=0,j=0,i+j\leq 3} \alpha_{ij}\mu_{ij}(t). \tag{11}$$

Next, introduce the system states $\boldsymbol{\nu}$ and $\boldsymbol{\mu}$:

$$\boldsymbol{\nu} = \begin{pmatrix} \nu_{00} & \nu_{01} & \cdots & \nu_{0p_2} \\ \nu_{10} & \nu_{11} & \cdots & \nu_{1p_2} \\ \vdots & \cdots & \ddots & \cdots \\ \nu_{p_1 0} & \nu_{p_1 1} & \cdots & \nu_{p_1 p_2} \end{pmatrix}, \quad \boldsymbol{\mu} = \begin{pmatrix} \mu_{00} & \mu_{01} & \cdots & \mu_{0w} \\ \mu_{10} & \mu_{11} & \cdots & \mu_{1w} \\ \vdots & \cdots & \ddots & \cdots \\ \mu_{v0} & \mu_{v1} & \cdots & \mu_{vw} \end{pmatrix}$$

and let the constant coefficients in the model (9) for $k = 1, 2$ referring to the coordinates λ_1 and λ_2, be collected in the corresponding matrices $\mathbf{B}_k$, $\mathbf{C}_k$, $\mathbf{D}_k$, and $\boldsymbol{\phi}_{0,k}$ as

$$\mathbf{B}_k = \begin{pmatrix} b_{00}^{(k)} & b_{10}^{(k)} & b_{20}^{(k)} & b_{30}^{(k)} \\ b_{01}^{(k)} & b_{11}^{(k)} & b_{21}^{(k)} & b_{31}^{(k)} \\ \vdots & \vdots & \vdots & \vdots \\ b_{0,p_k}^{(k)} & b_{1,p_k}^{(k)} & b_{2,p_k}^{(k)} & b_{3,p_k}^{(k)} \end{pmatrix}, \mathbf{C}_k = \begin{pmatrix} 0 & c_{10}^{(k)} & \cdots & c_{p_k,0}^{(k)} \\ 0 & 0 & \cdots & c_{p_k,1}^{(k)} \\ \vdots & \vdots & \ddots & \vdots \\ 0 & 0 & \cdots & c_{p_k,p_k-1}^{(k)} \\ 0 & 0 & \cdots & 0 \end{pmatrix},$$

$$\mathbf{D}_k = \begin{pmatrix} d_{00}^{(k)} & d_{10}^{(k)} & \cdots & d_{p_k,0}^{(k)} \\ d_{01}^{(k)} & d_{11}^{(k)} & \cdots & d_{p_k,1}^{(k)} \\ \vdots & \vdots & \ddots & \vdots \\ d_{0,p_k}^{(k)} & d_{1,p_k}^{(k)} & \cdots & d_{p_k,p_k}^{(k)} \end{pmatrix}, \quad \boldsymbol{\phi}_{0,k} = \begin{pmatrix} \phi_{0,k}(0) \\ \phi_{1,k}(0) \\ \vdots \\ \phi_{(p_k,k)} \end{pmatrix}^T.$$

Then, the ODEs regarding the evolution of the states can be stated in the following compact form:

$$\dot{\boldsymbol{\nu}} = \mathbf{C}_1\boldsymbol{\nu}\, G_{0,1}\big(u,\boldsymbol{\mu}\big) + \boldsymbol{\nu}\,\mathbf{C}_2^T G_{0,2}\big(u,\boldsymbol{\mu}\big) + B\big(u,\boldsymbol{\mu}\big)\boldsymbol{\phi}_{0,1}\boldsymbol{\phi}_{0,2}^T - \mathbf{D}_1\boldsymbol{\nu}\,\mathbf{D}_2^T, \tag{13a}$$

with the output equation given by

$$\boldsymbol{\mu} = \mathbf{B}_1\boldsymbol{\nu}\,\mathbf{B}_2^T. \tag{13b}$$

An important special case with

$$B\big(u,\boldsymbol{\mu}\big) = B_0\big(u\big)V_C\big(\boldsymbol{\mu}\big), \tag{13c}$$

arises from modeling the secondary nucleation in crystallization, where existing particles promote the nucleation of the nuclei. From (11) it follows that with appropriate matrices $\mathbf{V}_{1C,i}$, $\mathbf{V}_{2C,i}$, the total volume V_C of the particle population may be written using the general expression

$$V_C(\boldsymbol{\mu}) = \sum_i \mathbf{V}_{1C,i}^T\,\boldsymbol{\mu}\,\mathbf{V}_{2C,i}, n \tag{13d}$$

It is important to observe that embedding the factor $\phi_i(\lambda)$ in (7) is essential for the closure of the above ODE-systems. Indeed, had one considered the approximation $h(\lambda) \approx \sum_{k=0}^{p} d_{k,0}\phi_k(\lambda)$ instead, then it would necessarily lead to an open ODE structure of unbounded order.

We emphasize also that due to the linearity of the underlying PDE (1), the distribution function $\tilde{f}$ can be decomposed as $\tilde{f} = \tilde{f}^{(\mathrm{n})} + \tilde{f}^{(\mathrm{s})}$, where the former summand represents the particular solution resulting from the birth-rate term B (and zero initial conditions, i.e., $\tilde{f}_0 \equiv 0$), and the latter one as the homogenous solution (invoked by the initial distribution $\tilde{f}_0$ and with $B \equiv 0$). In other words, $\tilde{f}_{\mathrm{n}}$ describes the density of the nuclei and $\tilde{f}_{\mathrm{s}}$ describes the evolution of the initial particle density $\tilde{f}_0$. As a consequence, one can associate to each the generalized moments $\nu_{kl}^{(\mathrm{n})}$ and $\nu_{kl}^{(\mathrm{s})}$, as well as the monomial moments $\mu_{ij}^{(\mathrm{n})}$ and $\mu_{ij}^{(\mathrm{s})}$.

3. LEAST SQUARE APPROXIMATION

Motivated by the deliberations in the previous section, here we resort briefly to computation of the approximations of terms $x^i(\lambda)$ and $h(\lambda)\phi_i(\lambda)$ in (7) in the least-square sense over a sequence of real orthogonal polynomials $\phi_0, \phi_1, \phi_2, etc$, where

$$\phi_k(\lambda) = \sum_{l=0}^{k} a_{kl}\lambda^l, \quad a_{kk} \neq 0 \quad (k = 0, 1, 2, etc). \tag{14}$$

In other words, we consider numerical solutions to the corresponding least-square fitting in discretized formulation:

$$\underset{\mathbf{b}_i}{\text{minimize}} \sum_{\ell=0}^{m} w_\ell \left(x^i(\lambda_\ell) - \sum_{k=0}^{p} b_{ki}\phi_k(\lambda_\ell) \right)^2 \tag{15a}$$

and

$$\underset{\mathbf{d}_i}{\text{minimize}} \sum_{\ell=0}^{m} w_\ell \left(h(\lambda_\ell)\phi_i(\lambda_\ell) - \sum_{k=0}^{p} d_{ki}\phi_k(\lambda_\ell) \right)^2, \tag{15b}$$

where $w_\ell > 0$ stands for the weights, and $\mathbf{b}_i := [b_{0i} \dots b_{pi}]$ and $\mathbf{d}_i := [d_{0i} \dots d_{pi}]$ collect the parameters which need to be estimated, and p and $\lambda_m = \lambda_{\max}$ are fixed. A numerically stable approach to solving the above least-square approximation problem exploits the orthogonality property of the polynomial sequence $\{\phi_k\}_{k=0}^{p}$. It is a well-known fact that the best approximating polynomial $\hat{x}^i(\lambda)$ of degree p for the given function $x^i(\lambda)$ is given by:

$$\hat{x}^i(\lambda) = \sum_{k=0}^{p} b_{ki}\phi_k(\lambda); \quad b_{ki} = \left\langle x^i(\lambda), \phi_k \right\rangle, \tag{16}$$

and, similarly, for $h(\lambda)\phi_i(\lambda)$,

$$h(\lambda)\phi_i(\lambda) = \sum_{k=0}^{p} d_{ki}\phi_k(\lambda); \quad d_{ki} = \langle h(\lambda)\phi_i,\, \phi_k \rangle. \tag{17}$$

According to the three-term recurrence formula (Björck, 1996), every sequence of triangular orthogonal polynomials $\{\phi_k\}_{k=0}^{p}$ can be associated with sequences of coefficients α_k, β_k and γ_k, $k = 0 \dots p$ fulfilling

$$\alpha_{k+1}\phi_{k+1} = (\lambda - \beta_k)\,\phi_k - \gamma_k\phi_{k-1}, \tag{18}$$

where α_{k+1} are non-zero reals, and, by convention, $\gamma_0 := 1$, $\phi_{-1}(\lambda) \equiv 0$, $\phi_0(\lambda) \equiv 1$. For sequences of monical polynomials $\{\phi_k\}_{k=0}^{p}$ it holds:

$$\alpha_{k+1} \equiv 1, \quad \beta_k = \frac{\langle \lambda\phi_k, \phi_k \rangle}{\langle \phi_k, \phi_k \rangle}, \quad \gamma_k = \frac{\langle \phi_k, \phi_k \rangle}{\langle \phi_{k-1}, \phi_{k-1} \rangle}. \tag{19}$$

The scheme (18) provides a recursive algorithm for construction of the orthogonal polynomials, where we consider the discrete inner product:

$$\langle \phi_k, \phi_l \rangle = \sum_{\ell=0}^{m} w_\ell\phi_k(\lambda_\ell)\,\phi_l(\lambda_\ell) \tag{20}$$

over a fixed grid of points. For simplicity, in computations we typically apply equidistant abscissas. Although in practice uniform weights are also often utilized (implying Gram polynomials), other weights may be more suitable for the specific application at hand. Indeed, our numerical examinations with the bivariate crystals in the next section indicate that the weights as defined in Table 2 outperform the uniform ones in terms of accuracy and stability.

4. A MOVING GRID DISCRETIZATION BASED NUMERICAL SCHEME

In this section, we describe an integration scheme used for comparison of results in the next section. It is based on the method of characteristics and a moving grid and is adapted from (Kumar and Ramkrishna, 1997) for the case of bivariate particles. Thereby, it is beneficial to consider the basic underlying model (1) in the transformed $\boldsymbol{\lambda}$-coordinates (2). In the following, to improve readability, the coordinates λ_1 and λ_2 are relabeled to x and y, i.e.:

$$x \triangleq \lambda_1, \quad \text{and} \quad y \triangleq \lambda_2.$$

The property space is discretized by means of rectangular bins, which are utilized in the region where $\tilde{f}(x,y,t)$ is non-zero. At any time, this region can be qualitatively separated into one part referring to the nuclei and denoted by the superscript (n), and another one, referring to the growing seed partciles, denoted by (s). It is then useful to define m bins referring to nucleation and another r bins referring to growing seeds.

The rectangular bins are constituted by their left and right, lower and upper boundaries. In the case of nucleation, the boundaries of the kth bin, $k \in \{1,\dots,m\}$, are denoted, respectively, as $x_k^{\prime(\mathrm{n})}$, $x_k^{\prime\prime(\mathrm{n})}$, $y_k^{\prime(\mathrm{n})}$, and $y_k^{\prime\prime(\mathrm{n})}$, and we allow these boundaries to lie outside of the physical domain (i.e., negative x and/or y). In the case of the growing seeds, the boundaries of the lth bin, $l \in \{1,\dots,r\}$, are denoted as $x_l^{\prime(\mathrm{s})}$, $x_l^{\prime\prime(\mathrm{s})}$, $y_l^{\prime(\mathrm{s})}$, and $y_l^{\prime\prime(\mathrm{s})}$. The goal is to keep track of the particle numbers $F_k^{(\mathrm{n})}$ and $F_l^{(\mathrm{s})}$ inside the bins, whereby it obviously holds:

$$F_k^{(\mathrm{n})}(t) = \int_{y_k^{\prime(\mathrm{n})}}^{y_k^{\prime\prime(\mathrm{n})}} \int_{x_k^{\prime(\mathrm{n})}}^{x_k^{\prime\prime(\mathrm{n})}} \tilde{f}(x,y,t)\,\mathrm{d}x\,\mathrm{d}y, \tag{21a}$$

$$F_l^{(\mathrm{s})}(t) = \int_{y_l^{\prime(\mathrm{s})}}^{y_l^{\prime\prime(\mathrm{s})}} \int_{x_l^{\prime(\mathrm{s})}}^{x_l^{\prime\prime(\mathrm{s})}} \tilde{f}(x,y,t)\,\mathrm{d}x\,\mathrm{d}y. \tag{21b}$$

Let the bin boundaries move with speeds $G_{0,1}(t)$ and $G_{0,2}(t)$ in x and y direction, respectively, i.e.:

$$\dot{x}_k^{\prime(\mathrm{n})} = G_{0,1}, \quad x_k^{\prime(\mathrm{n})} \geq 0, \quad \dot{y}_k^{\prime(\mathrm{n})} = G_{0,2}, \quad y_k^{\prime(\mathrm{n})} \geq 0, \tag{22a}$$

$$\dot{x}_k^{\prime\prime(\mathrm{n})} = G_{0,1}, \quad x_k^{\prime\prime(\mathrm{n})} \geq 0, \quad \dot{y}_k^{\prime\prime(\mathrm{n})} = G_{0,2}, \quad y_k^{\prime\prime(\mathrm{n})} \geq 0, \tag{22b}$$

$$\dot{x}_l^{\prime(\mathrm{s})} = G_{0,1}, \quad x_l^{\prime(\mathrm{s})} \geq 0, \quad \dot{y}_l^{\prime(\mathrm{s})} = G_{0,2}, \quad y_l^{\prime(\mathrm{s})} \geq 0, \tag{22c}$$

$$\dot{x}_l^{\prime\prime(\mathrm{s})} = G_{0,1}, \quad x_l^{\prime\prime(\mathrm{s})} \geq 0, \quad \dot{y}_l^{\prime\prime(\mathrm{s})} = G_{0,2}, \quad y_l^{\prime\prime(\mathrm{s})} \geq 0, \tag{22d}$$

and let

$$\Delta_k^{(\mathrm{n})}(t) := \int_{y_k^{\prime(\mathrm{n})}}^{y_k^{\prime\prime(\mathrm{n})}} \int_{x_k^{\prime(\mathrm{n})}}^{x_k^{\prime\prime(\mathrm{n})}} \delta(x)\delta(y)\,\mathrm{d}x\,\mathrm{d}y,$$

i.e.,

$$\Delta_k^{(\mathrm{n})}(t) = \begin{cases} 1, & 0 \in \left(x_k^{\prime(\mathrm{n})}, x_k^{\prime\prime(\mathrm{n})}\right], 0 \in \left(y_k^{\prime(\mathrm{n})}, y_k^{\prime\prime(\mathrm{n})}\right], \\ 0, & \text{otherwise.} \end{cases} \tag{23}$$

Then, it can be shown that the particle numbers evolve as

$$\begin{aligned} \dot{F}_k^{(\mathrm{n})} &= -\int_{y_k^{\prime(\mathrm{n})}}^{y_k^{\prime\prime(\mathrm{n})}} \int_{x_k^{\prime(\mathrm{n})}}^{x_k^{\prime\prime(\mathrm{n})}} h_1(x)h_2(y)\tilde{f}(x,y,t)\mathrm{d}x\mathrm{d}y + B(t)\Delta_k^{(\mathrm{n})}(t), \\ \dot{F}_l^{(\mathrm{s})} &= -\int_{y_l^{\prime(\mathrm{n})}}^{y_l^{\prime\prime(\mathrm{n})}} \int_{x_l^{\prime(\mathrm{n})}}^{x_l^{\prime\prime(\mathrm{n})}} h_1(x)h_2(y)\tilde{f}(x,y,t)\mathrm{d}x\mathrm{d}y. \end{aligned} \tag{24}$$

To integrate (24), we make the approximation that all particles within bins are concentrated at certain (moving) interior points with coordinates $x_k^{(\mathrm{n})}(t)$, $y_k^{(\mathrm{n})}(t)$, (nuclei) and $x_l^{(\mathrm{s})}(t)$, $y_l^{(\mathrm{s})}(t)$ (for seeds) lying somewhere inside the corresponding bins, i.e.,

$$\begin{aligned} \tilde{f}(x,y,t) \approx \textstyle\sum_{k=1}^{m} F_k^{(\mathrm{n})}(t)\delta(x_k^{(\mathrm{n})}(t))\delta(y_k^{(\mathrm{n})}(t)) \\ + \textstyle\sum_{l=1}^{r} F_l^{(\mathrm{s})}(t)\delta(x_l^{(\mathrm{s})}(t))\delta(y_l^{(\mathrm{s})}(t)). \end{aligned} \tag{25}$$

Note that the setting:

$$\dot{x}_k^{(\mathrm{n})} = G_{0,1}, \quad x_k^{(\mathrm{n})} \geq 0, \quad \dot{y}_k^{(\mathrm{n})} = G_{0,2}, \quad y_k^{(\mathrm{n})} \geq 0, \tag{26a}$$

$$\dot{x}_l^{(\mathrm{s})} = G_{0,1}, \quad x_l^{(\mathrm{s})} \geq 0, \quad \dot{y}_l^{(\mathrm{s})} = G_{0,2}, \quad y_l^{(\mathrm{s})} \geq 0, \tag{26b}$$

ensures that the interior particles never leave the bin in which they appear at $t = 0$, this implying:

$$\dot{F}_k^{(\mathrm{n})} \approx -h_1(x_k^{(\mathrm{n})})\,h_2(y_k^{(\mathrm{n})})\,F_k^{(\mathrm{n})}(t) + \Delta_k^{(\mathrm{n})}(t), \tag{27a}$$

$$\dot{F}_l^{(\mathrm{s})} \approx -h_1(x_l^{(\mathrm{s})})\,h_2(y_l^{(\mathrm{s})})\,F_l^{(\mathrm{s})}(t). \tag{27b}$$

If the bins are non-overlapping, approximations for integral properties of the distribution function, like the mixed moments or the net volumes $V_{C,\mathrm{n}}$ and $V_{C,\mathrm{s}}$ (which need to be computed due to their intrinsic feedback on nucleation and growth rates), can easily be obtained in a similar manner, e.g., when $\eta(x,y)$ is the volume of a single particle, $V_{C,\mathrm{n}} \approx \sum_{k=1}^{m} F_k^{(\mathrm{n})}(t)\eta(x_k^{(\mathrm{n})}(t), y_k^{(\mathrm{n})}(t))$. Note that only $r+2$ state variables are required to describe the evolution of the bins referring to the seed part of the PSD: r particle numbers plus two displacement variables $\tau_1(t) = \int_0^t d\xi$ and $\tau_2(t) = \int_0^t d\xi$; the positions of the bin interior points are $x_l^{(\mathrm{s})}(t) = x_l^{(\mathrm{s})}(0)+\tau_1(t)$, $y_l^{(\mathrm{s})}(t) = x_l^{(\mathrm{s})}(0)+\tau_2(t)$, and analogous expressions hold for the bin boundaries.

The variables are initialized as follows. A given initial distribution $\tilde{f}_0 = \gamma_1\gamma_2 f_0$ is covered by an $a \times b$-grid of bins, where $r = ab$, and the initial particle numbers are approximated as

$$\begin{aligned} F_l^{(\mathrm{s})}(0) = \tfrac{1}{4}\left(x_l^{\prime\prime(\mathrm{s})} - x_l^{\prime(\mathrm{s})}\right)\left(y_l^{\prime\prime(\mathrm{s})} - y_l^{\prime(\mathrm{s})}\right) \times \Big(\tilde{f}_0(x_l^{\prime(\mathrm{s})}, y_l^{\prime(\mathrm{s})}) \\ + \tilde{f}_0(x_l^{\prime(\mathrm{s})}, y_l^{\prime\prime(\mathrm{s})}) + \tilde{f}_0(x_l^{\prime\prime(\mathrm{s})}, y_l^{\prime(\mathrm{s})}) + \tilde{f}_0(x_l^{\prime\prime(\mathrm{s})}, y_l^{\prime\prime(\mathrm{s})})\Big). \end{aligned}$$

Furthermore, the m nucleation bins are initialized as

$$\begin{aligned} x_k^{\prime(\mathrm{n})}(0) = y_k^{\prime(\mathrm{n})}(0) = \tfrac{k-m-1}{m}\,\tfrac{\sqrt{2}}{2}\lambda_{\max}, \\ x_k^{\prime\prime(\mathrm{n})}(0) = y_k^{\prime\prime(\mathrm{n})}(0) = \tfrac{k-m}{m}\,\tfrac{\sqrt{2}}{2}\lambda_{\max}, \end{aligned}$$

where $\lambda_{\max}$ is an *a priori* assumed maximal possible length in the transformed property space (c.f. Table 2) of the nucleation locus on the basis of known maximum displacement variables $\tau_{1,\max}$, $\tau_{2,\max}$. The bin interior particles are also initially placed at the bin centers. Then, moving the negative nucleation bin boundaries and bin centers in accordance with

$$\begin{aligned} \dot{x}_k^{\prime(\mathrm{n})} = \|G_0\|,\ x_k^{\prime(\mathrm{n})} < 0,\ \dot{y}_k^{\prime(\mathrm{n})} = \|G_0\|,\ y_k^{\prime(\mathrm{n})} < 0, \\ \dot{x}_k^{\prime\prime(\mathrm{n})} = \|G_0\|,\ x_k^{\prime\prime(\mathrm{n})} < 0,\ \dot{y}_k^{\prime\prime(\mathrm{n})} = \|G_0\|,\ y_k^{\prime\prime(\mathrm{n})} < 0, \\ \dot{x}_k^{(\mathrm{n})} = \|G_0\|,\ x_k^{(\mathrm{n})} < 0,\ \dot{y}_k^{(\mathrm{n})} = \|G_0\|,\ y_k^{(\mathrm{n})} < 0, \end{aligned}$$

where $1 \leq k \leq m$, ensures that at any time exactly one bin contains the origin and, therefore, absorbs the nucleation term, and that the nucleation interior points have to pass the origin and therefore lie on the nuclei locus. The size of a bin can change as long as it contains the origin.

5. NUMERICAL EVALUATION

The proposed scheme shall now be numerically evaluated on a case-study with a bivariate batch crystallization process. In Section 2 we already emphasized that therefore an auxiliary dynamics is required to couple to the proposed ODE scheme (9), leading to algebraic feedback expressions in the form (6). The fundamental force for crystallization from the solution arises effectively from the relative level of supersaturation σ, which is a measure of the difference

between the solution concentration (or mass fraction) c and saturation concentration ($c_{\rm sat}$):

$$\sigma = c/c_{\rm sat} - 1 \text{ with } c = m_{\rm c}/(m_{\rm w} + m_{\rm c}), \tag{28a}$$

where $m_{\rm w}$ is the solvent and $m_{\rm c}$ the solute mass. The saturation concentration $c_{\rm sat}$ is fixed by the temperature T according to the empirical model $c_{\rm sat} = a_0 + a_1 T + a_2 T^2$. The nucleation rate B and the growth rates $G_{0,1}$ and $G_{0,2}$ are driven by the supersaturation level according to

$$B = k_b \sigma^b V_C, \quad G_{01} = k_{g_1} \sigma^{g_1}, \quad G_{02} = k_{g_2} \sigma^{g_2}, \tag{28b}$$

where k_{g_1}, g_1, k_{g_2}, g_2, k_b and b are empirical kinetic parameters. The solute consumption is described by the mass-balance law:

$$c(t) = c_0 - \rho(V_C(t) - V_{C,0}), \tag{28c}$$

where ρ_c is the mass density of crystal particles, and c_0, $V_{C,0}$ refer to the initial conditions. Finally, the expressions (6) result now directly by combining the latter equations, whereby u refers to the temperature T.

The problem data collected in Table 1 correspond to the crystallization of KDP (KH_2PO_4) dissolved in water. Notice that the data are defined with respect to the solvent mass. They are originally borrowed from (Ma et al., 2002) and also utilized in our previous work, (e.g., Bajcinca et al., 2014, and the references therein). Note that this model has size-independent growth rates, i.e. $\gamma_1(x_1) = \gamma_2(x_2) = 1$, as our primary focus here lies on the intricacies caused by the filtering term $h(x_1, x_2)$.

We examine four different simulations case-studies of a batch process, which are designed to cover a wide range of operation conditions regarding time-scale, relative ratio of nucleation to seed mass, and control policies. The first two, hosted in Fig. 1 and Fig. 2, refer to the case with $h(x_1, x_2) \equiv 0$, while Fig. 3 and Fig. 4 include the simulations with non-zero $h(x_1, x_2) = h_1(x_1)h_2(x_2)$, where the filtering factors $h_i(x_i)$, $i = 1, 2$, are specified in Table 2. Hereby we also list the weights w_ℓ and the least-square parameters p_i and m_i, c.f. Eq. (15). The plots are organized as follows. We show the total number of nucleated crystals ($\mu_{00}^{(\rm n)}$, top left diagrams) and the total volumes of the nucleation ($V_{C,\rm n}$, top right) and the growing seeds ($V_{C,\rm s}$, bottom right).

For comparison purposes, the simulation results corresponding to our proposed method (indicated by POL see Section 2) and those corresponding to the moving grid discretized numerical scheme (MOC) are plotted in the same diagrams. Note that, while in many cases the plotted curves virtually coincide, their individual presence is indicated by the respective (superimposed) marker symbols. The bottom left diagrams reflect the process in the property space. Note that target locations A and B are lying on the same, dash-dotted, equivolume curve (see the explanation below). The depicted path is traversed by the center of the growing seeds distribution according to the POL and MOC simulations. Furthermore, the MOC simulation yields information on the nucleation PSD at final time. The latter is illustrated by bars branching off the nucleation loci and pointing upwards resp. downwards, effectively forming shaded areas. The base points mark the positions $\mathbf{x}_k$ of the bin centers and the lengths indicate the net (estimated) masses $M_k = \rho_c \eta(\mathbf{x}_k) F_k$, with $\eta(\mathbf{x}) = x_1^2 x_2 - \frac{2}{3} x_1^3$, of nuclei in the respective bins (according to the provided scale). For details on the evolution of the momentary nuclei locus the reader is referred to Fig. 1 in (Bajcinca et al., 2014). Level sets are depicted for the initial seed distribution, and, in the cases with fines dissolution, also for the filtering function $h(x_1, x_2)$, i.e., $h(x_1)h(x_2) = \text{const}$.

We specify the desired shape in terms of the center of the narrow growing seeds distribution, which is initially located at $\mathbf{x}_{\rm ref,0}$. Two target locations $\mathbf{x}_{\rm ref,des}$, A and B, are selected for this case study in the following way. For constant temperature control (i.e., isothermal operation), the process simulations exhibit near-equilibirum conditions after 120 minutes. The temperature T is chosen such that in this equilibrium the volume of the grown seeds has converged to a prescribed value $V_{C,\rm s} = 6.1\,[\text{mm}^3/g_{\rm solv}]$. Without fines dissolution ($h \equiv 0$), this requires $T = 27.447\,[^\circ\text{C}]$ and the seed distribution center converges to target A. When the fines dissolution is in operation, the temperature has to be adjusted to $T = 30.78\,[^\circ\text{C}]$, resulting in the convergenve to target B. We also perform simulations for the isothermal operation of the process without fines dissolution at $T = 30.78\,[^\circ\text{C}]$, and operation with fines dissolution at $T = 27.447\,[^\circ\text{C}]$. In these "mismatched" cases, the final seed volume misses the prescribed value $V_{C,\rm s} = 6.1\,[\text{mm}^3/g_{\rm solv}]$ by undershooting (see Fig. 2) or overshooting (see Fig. 3) it. Moreover, we perform simulations for the case of constant supersaturation control (which can be shown to minimize the batch time) aiming at target A or B. Several remarks are now of order.

(i) Apart from some small errors in simulations with non-zero filtering h-factor (e.g. in μ_{00} in Fig. 3), the accuracy of our scheme (POL) matches very tightly to that of the discretized model scheme (MOC) in all conditions and simulation scenarios. Hereby, we apply least-square fitting in Eq. (15) with $p_1 = p_2 = 22$ and for the discretization scheme about: 300 bins with $\lambda_{1,\max} = 0.5$mm and $\lambda_{2,\max} = 1$mm. Consequently, the order of our ODE scheme is $2 \times 23 \times 23 = 1058$, while that of the moving grid scheme is $2 \times 3 \times 300 = 1800$.

(ii) It can be shown that the trajectories corresponding to the scenario with constant supersaturation are generally time-optimal. Now, a comparison of the bar plots of Figs. 1 and 3 with A as the final location, and Figs. 2 and 4 with B as the final location, indicates a lower amount of the resulting nuclei in cases with fines removal due to the non-zero h-term. These outcomes are, of course, a consequence of the dissolution and they are also visible in the top-right plots corresponding to the nuclei volume $V_{C,\rm n}$.

(iii) It is interesting to observe that small deviations of the destination point (i.e. A and B) in the property space are associated with large changes in the corresponding required optimal times; c.f. the plots of Figs. 1 and 2 (as well as those in Figs. 3 and 4).

(iv) Comparison of the two figures involving fines removal (i.e. h-term) reveals that in both control scenarios (i.e. with constant temperature and supersaturation), the location A is reached in a very short time at the cost of large nuclei mass content, while reaching the location B takes considerably longer, however at a negligible amount of nuclei mass. This illustrates the trade-off between the process duration and nuclei content. In other words, shorter processes imply larger impurity and vice-versa. In fact, such situations are present in all batch crystallization processes (see, e.g., the previous contributions of the authors in the area, such as (Bajcinca, 2013) and the references therein).

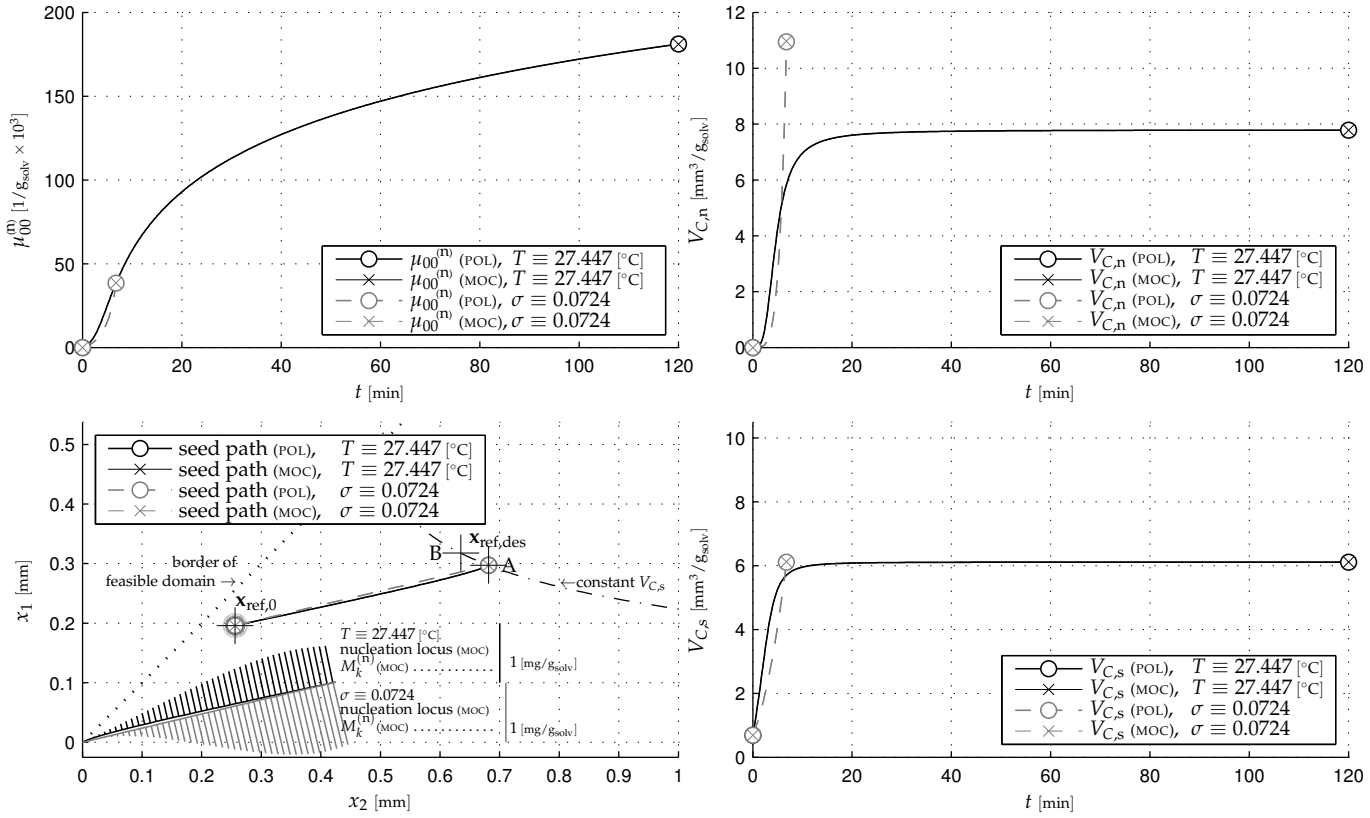

Figure 1. No fines dissolution ($h = 0$). Constant temperature and supersaturation excitation. Isothermal excitation tuned to reach the equilibirum location A.

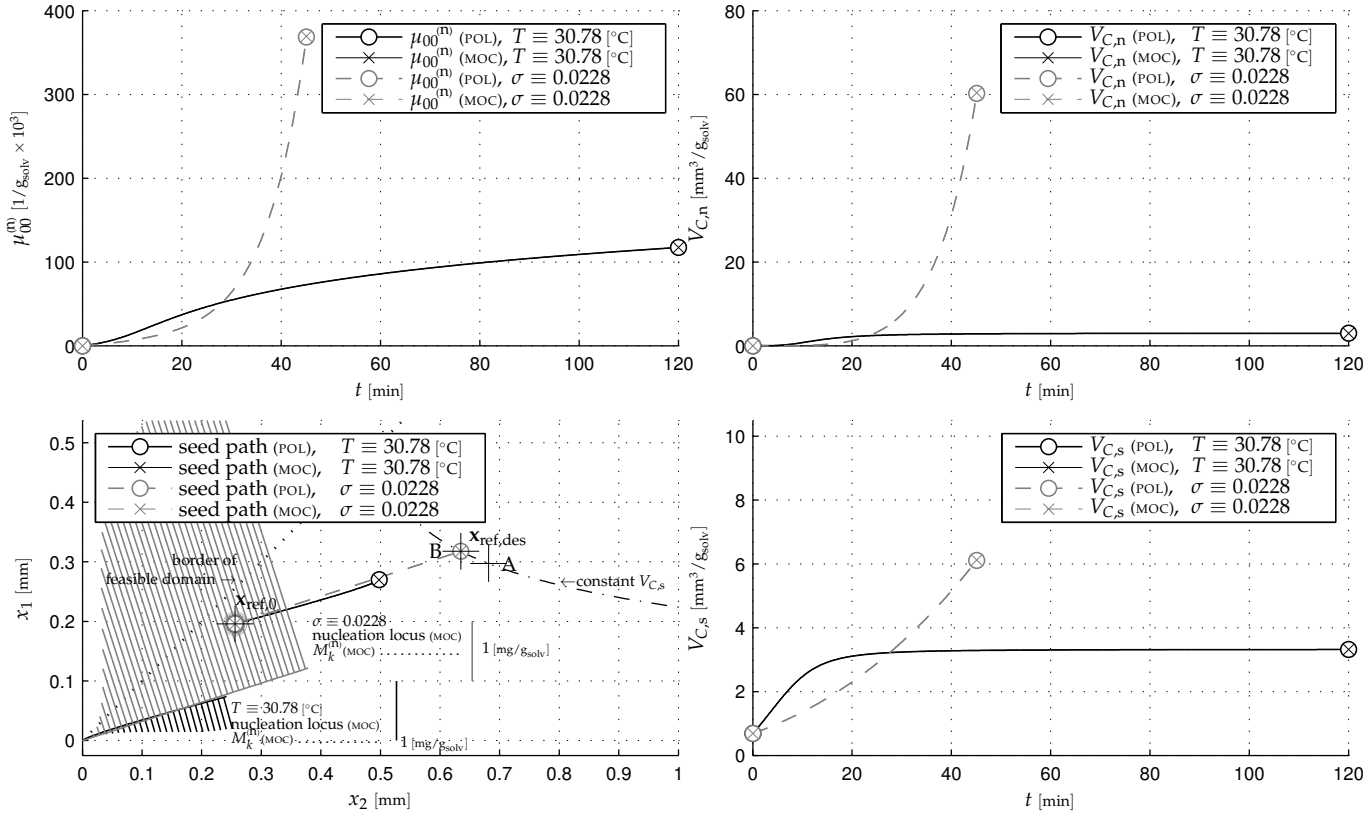

Figure 2. No fines dissolution ($h = 0$). Isothermal excitation tuned in Fig. 3 (to equilibrium location B) captured here at an earlier equilibirum location on its way to the final destination B.

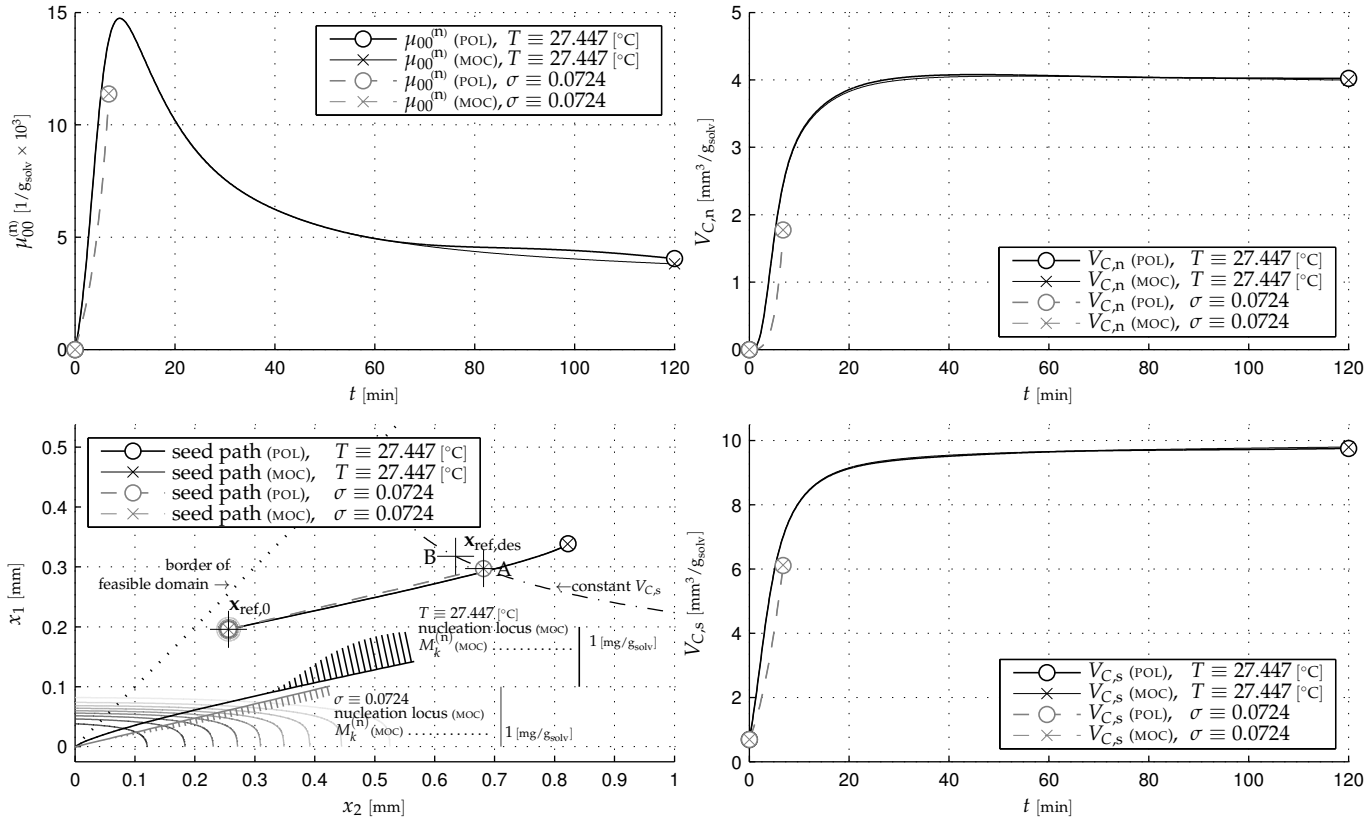

Figure 3. Illustrating the fines dissolution. Equilibirum under the isothermal excitation (tuned in Fig. 1) lies beyond the final destination A.

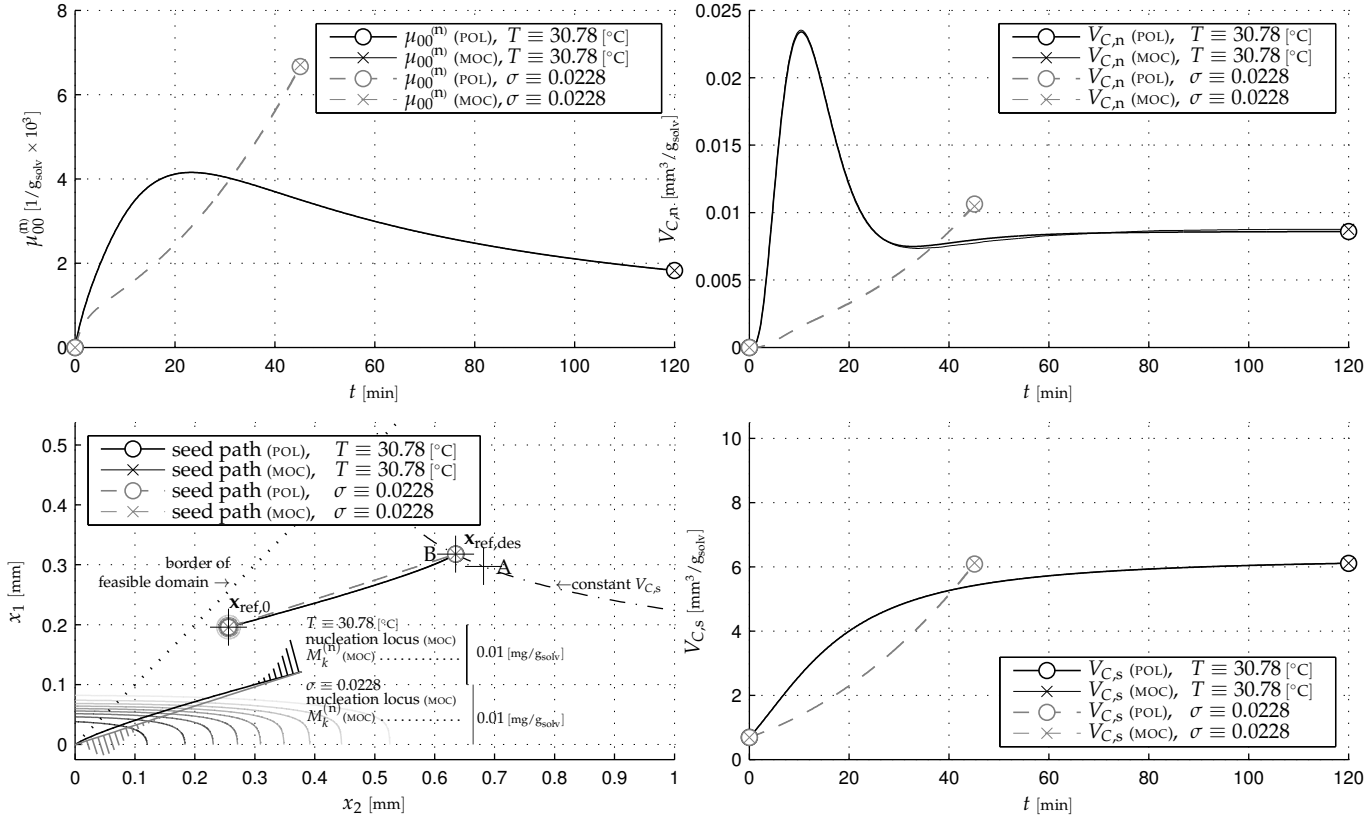

Figure 4. Illustrating the action of fines dissolution due to the non-zero decaying h-term. Constant temperature and supersaturation excitation. Isothermal excitation tuned to reach the equilibirum final destination B.

Table 1.

Parameter description	*Symbols*	*Value*
growth rate constant	k_{g_1}	12.1×10^{-6} m/s
growth rate constant	k_{g_2}	100.75×10^{-6} m/s
nucleation rate constant	k_b	7.49×10^{10} $1/m^3 s\ g_{solv}$
growth rate exponent	g_1	1.48
growth rate exponent	g_2	1.74
nucleation rate exponent	b	0.51
density of crystals	ρ	2340 kg/m^3
1st solubility parameter	a_0	0.2087
2nd solubility parameter	a_1	-9.7629×10^{-5} $1/°C$
3rd solubility parameter	a_2	9.3027×10^{-5} $1/°C^2$
Filtering term	$h(\mathbf{x}) = h_1(x_1) \times h_2(x_2)$	
$h_i(x_i) = k_{h,i}(1-(1+\exp(-m_{h,i}(x_i - x_{h,i})))^{-1})$		
$k_{h,1} = k_{h,2} = \sqrt{0.01 \times 1/s}$, $x_{h,1} = 0.06\,mm$, $x_{h,2} = 0.3\,mm$		
$m_{h,1} = 100 \times 1/mm$, $m_{h,2} = 10 \times 1/mm$		
Initial conditions		
initial seed volume	$V_{C,0}$	$0.6879\,mm^3/g_{solv}$
initial seed mass	m_{seed}	$1.6\,mg/g_{solv}$
initial mass fraction	c_0	0.307
initial seed PSD	$x_{1,0} = 0.196\,mm$, $x_{2,0} = 0.256\,mm$	
$a = -3.479 \times 10^8\ 1/(g_{solv}\,mm^4)$, $b = 1.781 \times 10^8\ 1/(g_{solv}\,mm^2)$		
$f_0(x_1, x_2) = \max\left[0,\ a\left((x_1 - x_{1,0})^2 + (x_2 - x_{2,0})^2\right) + b\right]$		

(v) Finally, we focus on interpretation of some interesting outcomes related to the isothermal control policies. The essentially larger nucleation masses as depicted in the pendant top-right plots of Figs. 1 and 3 result from the different levels of the isothermal excitation at $T = 27.447°C$ (in Fig. 3) and $T = 30.78°C$ (in Fig. 4). This implies more intensive nucleation and growth of the particles in the beginning of the process excited by a lower temperature in Fig. 3. As a result, a large amount of particles manages to cross fast over the dissolving area occupied by the filtering h-term in Fig. 3. This is clearly indicated in the bottom-left plot of Fig. 3, whereby the seed particles considerably miss the destination location A by landing at another equilibirum location beyond, i.e. they grow at larger sizes than those in the pendant top-left plot in Fig. 1. It is interesting to observe that because of this condition, the same order of the available nuclei particles at the end of the batch (c.f. pendant top-left plots corresponding to μ_{00} of Figs. 3 and 4) produce quite different order levels of the nuclei mass. We, finally, remark that the isothermal scenario in Fig. 4 demonstrates the accurate operability of our scheme under diverse conditions within a single operational mode.

CONCLUSION

In this work we introduce an ODE modeling structure for a special class of the PDE systems arising in particulate systems. The proposed scheme represents an extension to the theory of the approximate methods of moments, which has been developed by authors in a series of previous papers. The specifics of the presented scheme focus on the impact of a filtering mechanism in a multivariate PDE, which, for instance, may amount to external fines removal in particulate systems. While in this article we focus on derivation of the ODE scheme and its verification by means of extensive numerical simulations, our results provide a useful basis for solving control and optimization problems for special classes of particulate processes with specific filtering and size-dependent growth rate dependencies.

Table 2.

Parameter description	*Symbols and values*
MOC moving grid model ($\lambda_1 = x_1$, $\lambda_2 = x_2$)	
Maximal	$x_{1,max} = 0.5 \times 10^{-3}$ m
particle dims.	$x_{2,max} = 1 \times 10^{-3}$ m
Boundaries of the	$(x^{(S)}_{1,min}, x^{(S)}_{1,max}) = (0.15, 0.23) \times 10^{-3}$ m
init. seed grid	$(x^{(S)}_{2,min}, x^{(S)}_{2,max}) = (0.21, 0.29) \times 10^{-3}$ m
Boundaries of the	$(x^{(n)}_{1,min}, x^{(n)}_{1,max}) = (-\sqrt{2}/2, 0) \times \lambda_{max}$
init. nucl. grid	$(x^{(n)}_{2,min}, x^{(n)}_{2,max}) = (-\sqrt{2}/2, 0) \times \lambda_{max}$
	$\lambda_{max} = x_{1,max} - x^{(S)}_{1,max} + x_{2,max} - x^{(S)}_{2,max}$
Number of bins	$m + r = 100 + 15 \times 15$
Polynomial moment model POL	
Maximum order	$p_1 = p_2 = 22$
No. of grid. pts.	$m_1 = m_2 = 1000$
Max. particle dims.	*see* MOC *settings*
Bound. seed PSD	*see* MOC *settings*
Weights for polyn.	$x_{\ell,i} = x_{i,max}\,\ell/(m_i - 1)$, $0 \le \ell \le m_i - 1$
constr., $i \in \{1, 2\}$	$w_{\ell,i} = (1/x^3_{1,i})^2$, $\ell = 0$
	$w_{\ell,i} = (1/x^3_{\ell,i})^2$, $1 \le \ell \le \ell_{h,i}$
	$w_{\ell,i} = (1/x^3_{\ell_{h,i},i})^2$, $\ell_{h,i} + 1 \le \ell \le m_i - 1$
	where $\ell_{h,i}$ is defined as the maximum ℓ such that $x_{\ell,i} < x_{h,i}$
Simulations with POL model and MOC model	
ODE solver	`ode45` (Matlab®),
Rel. and abs. tol.	1×10^{-6}
Max. step size	10 sec

ACKNOWLEDGEMENTS

We gratefully acknowledge the financial support of this work by the German Research Foundation (DFG) under the grants SU-189/5-1 and RA 516/9-1.

REFERENCES

Bajcinca, N., Hofmann, S., and Sundmacher, K. (2014). Method of moments over orthogonal polynomial bases. *Chemical Engineering Science*, 119(0), 295–309.

Bajcinca, N. (2013). Analytic solutions to optimal control problems in crystal growth processes. *Journal of Process Control*, 23, 224–241.

Björck, Å. (1996). *Numerical Methods for Least Squares Problems*. Society for Industrial and Applied Mathematics (SIAM).

Koren, B. (1993). A robust upwind discretisation method for advection, diffusion and source terms. *Numerical Methods for Advection-Diffusion Problems*, 117–138.

Kumar, S. and Ramkrishna, D. (1997). On the solution of population balance equations by discretization–III. Nucleation, growth and aggregation of particles. *Chemical Engineering Science*, 52(24), 4659–4679.

Ma, D.L., Tafti, D.K., and Braatz, R.D. (2002). Optimal control and simulation of multidimensional crystallization processes. *Computers & Chemical Engineering*, 26, 1103–1116.

Qamar, S., Elsner, M.P., Angelov, I., Warnecke, G., and Seidel-Morgenstern, A. (2006). A comparative study of high resolution schemes for solving population balances in crystallization. *Computers & Chemical Engineering*, 30(6-7), 1119–1131.

Ramkrishna, D. (2000). *Population Balances: Theory and Applications to Particulate Systems in Engineering*. Academic Press, A Harcourt Science and Technology Company, second edition.